Journal of Power Sources 196 (2011) 8091–8097

Contents lists available at ScienceDirect

Journal of Power Sources

journal homepage: www.elsevier.com/locate/jpowsour

Electrochemical behaviors of a Li_3N modified Li metal electrode in secondary lithium batteries

Meifen Wu, Zhaoyin Wen*, Yu Liu, Xiuyan Wang, Lezhi Huang

CAS Key Laboratory of Materials for Energy Conversion, Shanghai Institute of Ceramics, Chinese Academy of Sciences, 1295 Ding Xi Road, Shanghai 200050, PR China

ARTICLE INFO

Article history:
Received 22 December 2010
Received in revised form 15 April 2011
Accepted 16 May 2011
Available online 27 May 2011

Keywords:
Lithium nitride
Li metal electrode
Batteries
Protective film

ABSTRACT

A lithium conductive Li_3N film is successfully prepared on Li metal surface by the direct reaction between Li and N_2 gas at room temperature. X-ray diffraction (XRD), Auger electron spectroscopy (AES), cyclic voltammetry (CV), scanning electron microscopy (SEM), AC impedance, cathodic polarization and galvanostatic charge/discharge cycling tests are applied to characterize the film. The experimental results show that the Li_3N protective film is tight and dense with high stability in the electrolyte. Its thickness is more than 159.4 nm and much bigger than that of a native SEI film formed on the lithium surface as received. An exchange current as low as 3.244×10^{-7} A demonstrates the formation of a complete SEI film at the electrode|electrolyte interface with Li_3N modification. The SEI film is very effective in preventing the corrosion of the Li electrode in liquid electrolyte, leading to a decreased Li|electrolyte interface resistance and an average short distance of 3.16×10^{-3} cm for Li ion diffusion from electrolyte to Li surface. The Li cycling efficiency depends on N_2 exposing time and is obviously enhanced by the Li_3N (1 h) modification. After cycling, a dense and homogeneous Li layer deposits on the Li_3N (1 h) modified Li surface, instead of a loose and inhomogeneous layer on the Li surface as received.

1. Introduction

Metallic lithium with a high theoretical specific capacity of 3860 A h kg^{-1} is a promising anode candidate for rechargeable Li batteries [1]. However, the practical application of Li electrode is still difficult due to its low cycling efficiency, deleterious dendritic morphology of deposited Li and safety concerns [2–4]. These problems have been widely believed to result from the reaction of freshly deposited Li with the electrolyte components such as solvents, Li solutes, and trace contaminants like water and oxygen [5–9]. A number of attempts have been made to improve the performance of Li electrodes by coating the Li with different kinds of surface protective films before or during cycling. Such protective films must conduct Li ions, and at the same time can prevent the contact between Li and electrolyte. One approach is to form a protective film by an in situ reaction between Li and the compounds, such as HF [10–13], $AlCl_3$, SnI_2 [14–16] and 2-methylfuran [17,18]. Most of such in situ films failed to protect the Li effectively due to their porous morphologies. Another approach is to make a pre-formed protective film by an *ex situ* route. For example, N. J. Dudney [19] and Visco et al. [20] fabricated stable Li electrodes by coating the Li surface with lithium phosphorus oxynitride ('LiPON') or related materials by sputtering. However, such a process is not favorable for commercial rechargeable Li batteries due to its high fabrication cost.

Owing to the limited Li ion conductivities of the above protective films, the interface resistance usually increased after the modifications. As known, polycrystalline Li_3N has an exceptionally high Li-ion conductivity (approximately 10^{-3} S cm^{-1}) with potential application as a solid electrolyte in lithium ion batteries [21]. In this work, a Li_3N film was fabricated on Li surface as a protective layer by the direct reaction between Li and N_2 gas at room temperature. The *ex situ* method proposed here is more effective and simpler compared with the methods such as sputtering or polymerizing. The protective film shows positive effects on the electrochemical behaviors of Li in a conventional organic electrolyte.

2. Experimental

In a designed container, one face of a fresh Li foil with thickness of 200 μm was allowed to flow N_2 gas at a constant space velocity for 1 h. The other side of the container was sealed by water-free liquid. A schematic diagram in Fig. 1 shows the detailed fabrication process. A Li electrode with Li_3N protective film was obtained. Then the modified Li foil was sealed by a polyimide film in order to prevent undesirable reactions during the test in air and was characterized by X-ray diffraction (XRD, Ultima IV) with Cu Kα radiation to identify the Li_3N phase formed. Auger Electron Spectroscopy (AES, Microlab 310 F) was used to examine the elements on the surface and within the Li_3N modified lithium electrode. An Ar ion

* Corresponding author. Tel.: +86 21 52411704; fax: +86 21 52413903.
E-mail addresses: zywen@mail.sic.ac.cn, liangxiao@student.sic.ac.cn (Z. Wen).

0378-7753/$ – see front matter © 2011 Elsevier B.V. All rights reserved.
doi:10.1016/j.jpowsour.2011.05.035

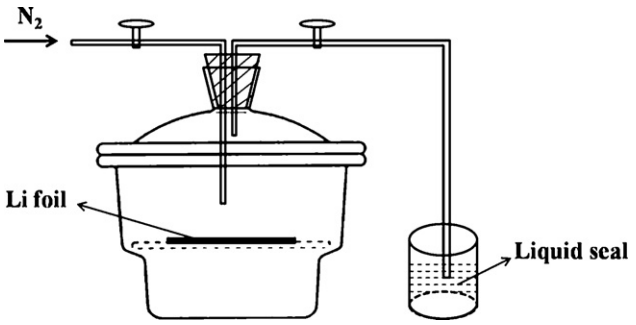

Fig. 1. A schematic diagram for the preparation process of Li_3N film on Li surface.

beam from a tungsten field emission gun with an etching rate of 0.1 nm s^{-1} was sputtered on to the sample with an incidence angle of 48 ± 1° in order to perform AES and the pressure during the measuring time was always lower than 1×10^{-7} Pa. All AES results were obtained from sample areas of 120 μm × 90 μm.

All electrochemical measurements were performed with sealed coin cells. Copper foils of 14 mm in diameter were used as working electrodes. Before the tests, the copper foil was polished to a mirror surface, washed with distilled water and acetone in an ultrasonic bath, and finally dried for 6 h under vacuum at room temperature. The working electrodes were assembled in 2025 coin cells using Celgard 2400 as the separators and Li foils as the counter and reference electrodes. A solution of 1 M $LiPF_6$ in EC:DMC (1:1 weight) was employed as the electrolyte. Cell assembling was processed in an argon filled glove box with oxygen and water contents less than 1 ppm.

AC impedance measurements were carried out using an Autolab PGSTAT302 potentiostat–galvanostat electrochemical workstation with a frequency response analyzer (FRA) software. The frequency and amplitude were set to 1 MHz–10 mHz and 10 mV, respectively. The cathodic polarization measurements for characterization of electrode kinetic performance were conducted on a CHI440 Electrochemical Workstation with a scan rate of 1 mV s^{-1}. The cyclic voltammetry measurements were monitored using Autolab PGSTAT302 potentiostat–galvanostat electrochemical workstation with general purpose electrochemical system (GPES) software. The cyclic potential was set to −0.4 to 0.8 V with a scan rate of 2 mV s^{-1}.

The galvanostatic charge/discharge tests were conducted on a LAND CT2001A battery test system. Li of 0.9 C cm^{-2} was deposited at the cycling current density of 0.5 mA cm^{-2}. The cut-off potential was controlled at 1 V (vs. Li/Li^+) for the Li dissolution. The Li cycling efficiency (Eff) was calculated using Eq. (1).

$$\text{Eff} = \frac{Q_{\text{dissolution}}}{Q_{\text{deposition}}} \times 100\% \quad (1)$$

where $Q_{\text{deposition}}$ was the charge quantity of Li deposition, $Q_{\text{dissolution}}$ was the dissolution quantity of deposited Li.

After the cycling efficiency test, the Li electrodes were removed from the coin cells, washed with polycarbonate (PC) and further dried in argon-filled glove-box for 12 h and were enclosed in a sealed sample holder to observe their morphologies with a scanning electron microscope (SEM, HITACHI S-3400).

3. Results and discussion

3.1. Physical characterization of Li_3N film

3.1.1. Phase analysis

The phase of Li_3N film formed on Li surface was characterized by XRD analysis. As shown in Fig. 2, the protective amorphous polyimide film displayed a broad band, no any sharp diffraction peaks owing to crystalline phases were seen. Fig. 2b shows the XRD pattern of the primitive Li foil. Three crystal peaks can be indexed to the Li metal. In addition, a small impurity peak was observed, probably due to minor oxidation of the Li metal during storage. Fig. 2c shows the typical pattern of the modified Li foil surface. As indicated, all peaks are indexed to Li_3N phase. No any impurity phase was found. It was also indicated that the minor surface impurity on the as-received Li foil did not influence the modification obviously. It is noticeable that there are two isomorphs of Li_3N with hexagonal structures, i.e., α-Li_3N [P6/mmm] and α′-Li_3N [P3m1] [22], respectively. As studied by Shouxin Cui, et al. [23], the transition from α-Li_3N to α′-Li_3N is very easy as the transition enthalpy barrier is only about 0.01 meV. In addition, the analysis of the density of states (DOS) and charge density distribution revealed that both α-Li_3N and α′-Li_3N have high Li ion conductivities. In order to investigate the stability of the formed Li_3N film in the electrolyte, we stored the modified Li foil in the same electrolyte for as long as three weeks and then dried it. The XRD pattern of the treated surface is shown in Fig. 2d. As certified, no phase change was caused by the treatment, indicating favorable thermodynamic stability of the Li_3N film in the electrolyte.

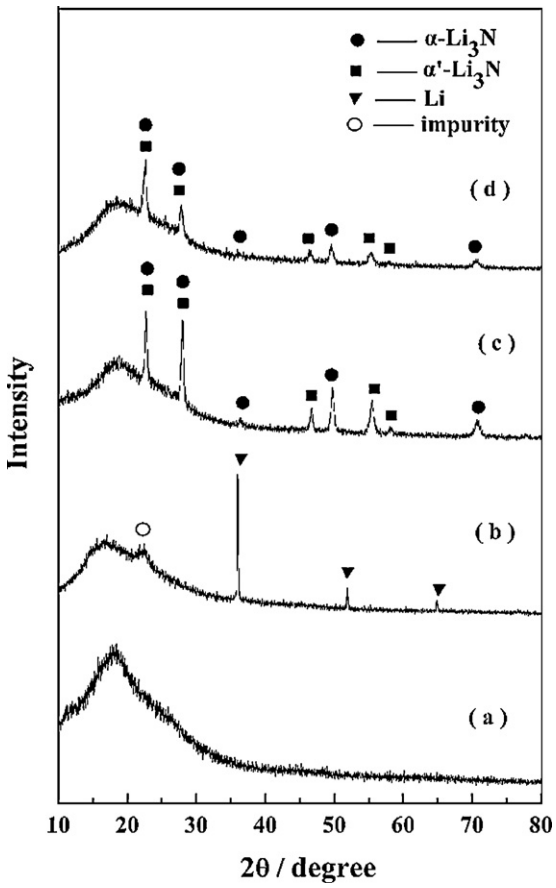

Fig. 2. XRD patterns of (a) protective polyimide film; (b) Li metal surface as received; (c) Li_3N (1 h) modified Li and (d) the Li_3N modified Li stored in the electrolyte for three weeks.

3.1.2. Surface components analysis

Fig. 3 shows the AES spectra of (a) Li 1s, (b) C 1s, (c) N 1s and (d) O 1s at different depths after N_2 flowed over Li surface for 1 h. Several depth profile spectra as shown in each figure were obtained by the argon ion etching for various periods with an incidence etching rate of 0.1 nm s^{-1}. At the depth of Li surface less than 10.4 nm, Li_2CO_3, Li_2O, LiOH and impurities were detected. A peak in Fig. 3(b)

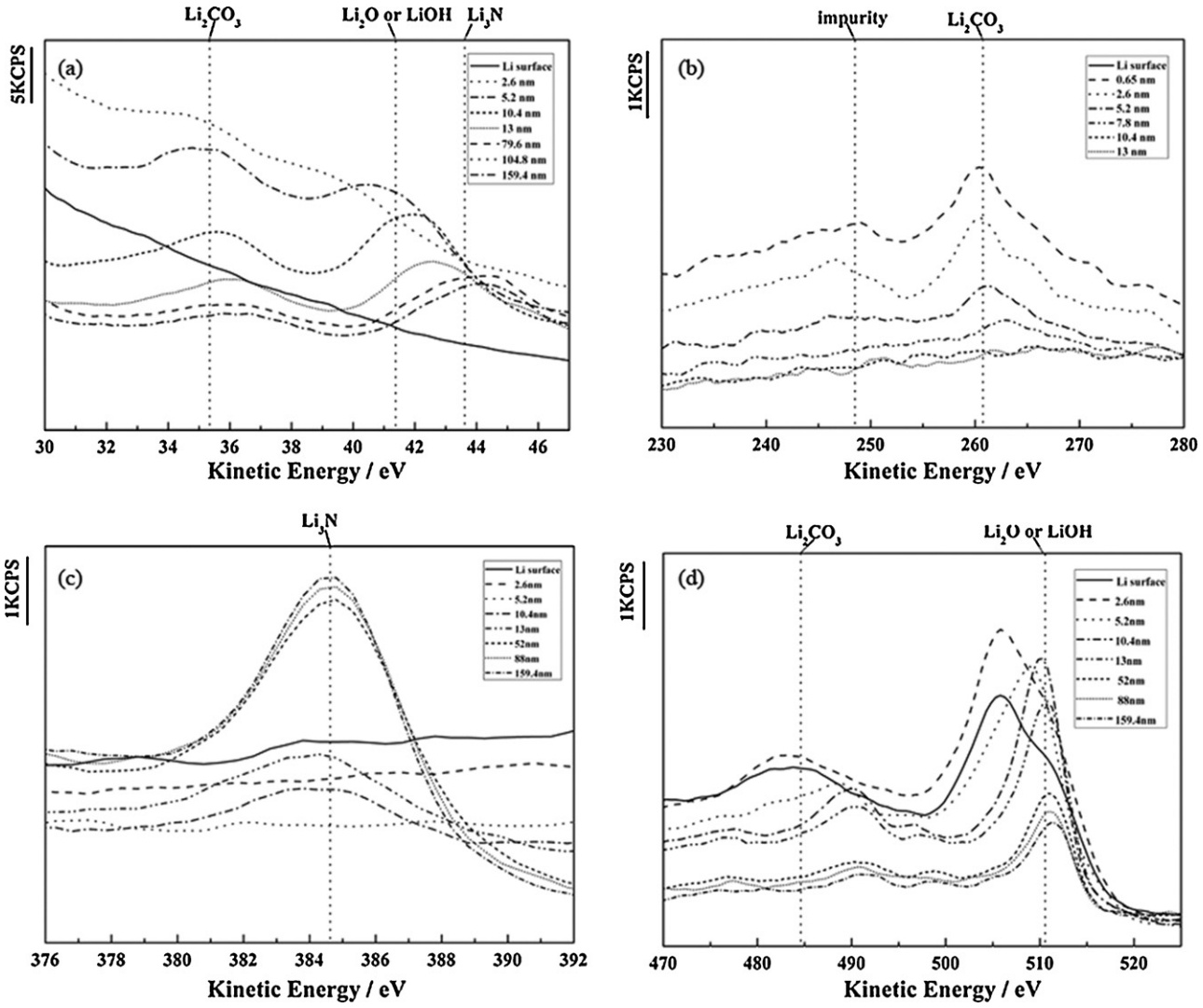

Fig. 3. AES spectra of (a) Li 1s; (b) C 1s; (c) N 1s; (d) O 1s on the Li_3N (1 h) modified Li surface.

at around 248 eV could be attributed to impurities since it quickly vanished at 7.8 nm with the argon ion etching. The Li_2CO_3 peak at around 260 eV disappeared at 13 nm. As Li_3N has a poor stability to humidity, it was not observed until 13 nm as shown in Fig. 3c. Two O peaks appeared at around 485 eV and 510 eV can be attributed to Li_2CO_3 and Li_2O or LiOH, respectively. Both of them were quickly decreased and finally kept at a low level at the depth larger than 52 nm. This is probably due to the trace humidity of the sputtering chamber and trance oxygen on Li. The thickness of Li_3N is more than 159.4 nm for exposing 1 h as shown in Fig. 3. It is much thicker than the native film formed on lithium as received.

3.2. Electrochemical performance of Li_3N modified Li electrode

3.2.1. Interface stability analysis

Fig. 4a and b shows typical Nyquist plots obtained from the as-received Li and Li_3N (1 h) modified Li electrodes as a function of storage time in $LiPF_6$/EC + DMC electrolyte. The inserts show the magnification of high frequency range of the impedance spectra. The equivalent circuit and related analogs fitted to the experimental data are also given in the spectra. A typical inductance element L identified by negative values in $-Z''$ axis indicates an unstable measurement system at the beginning [24]. The first depressed semicircle at high frequency can be attributed to migration resistance R_f of Li^+ through the surface film. According to the studies by Aurbach et al. [25–27], the different volume of each reduced species from $LiPF_6$/EC + DMC electrolyte, such as LiF, Li_xPF_y, $Li_xPF_yO_2$, $(CH_2OCO_2Li)_2$, CH_3OCO_2Li, CH_3OLi, etc. precipitated on the electrode [28], results in a rather rough and inhomogeneous surface film. For such case, the surface film capacitance is expressed by a constant phase angle element Q_f. The impedance of Q_f is written as Eq. (2)

$$Z_{Q_f} = Y_0^{-1}(j\omega)^{-n} \tag{2}$$

where ω is the angular frequency in rad s^{-1}, Y_0 is the magnitude of Q_f which can be approximately converted into a capacitance, and n is introduced to represent the deviation from the ideal RC-behavior which can vary between 1 for a pure capacitance, 0.5 for a Warburg resistance, and 0 for a pure resistor [29]. For intermediate values of n, Q_f may represent a film growth process taking place prevalently through a finite diffusion length [30]. The second semicircle in the low frequency region, which is represented by 'Cothyperbol' element O, suggests that a stagnant layer of finite length is formed in the electrolyte for Li^+ diffusion. The impedance of O is written as Eq. (3)

$$Z_O = Y_0^{-1}(j\omega)^{-1/2}\ \tanh[B(j\omega)^{1/2}] \tag{3}$$

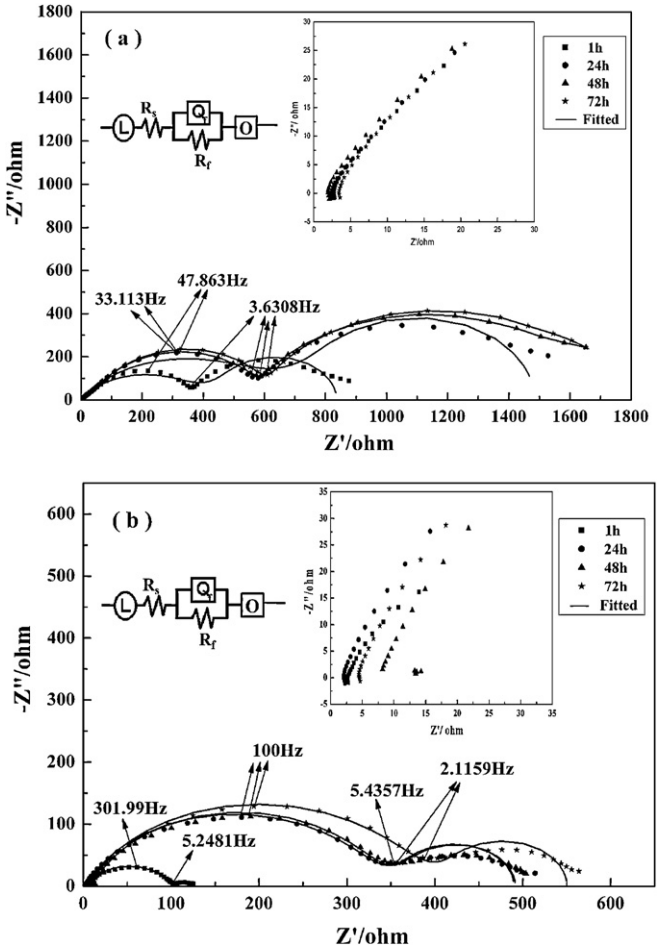

Fig. 4. Nyquist plots and the related equivalent circuit analogs for the Li as received (a) and Li_3N (1 h) modified Li electrodes (b) measured at open-circuit potential as a function of storage time.

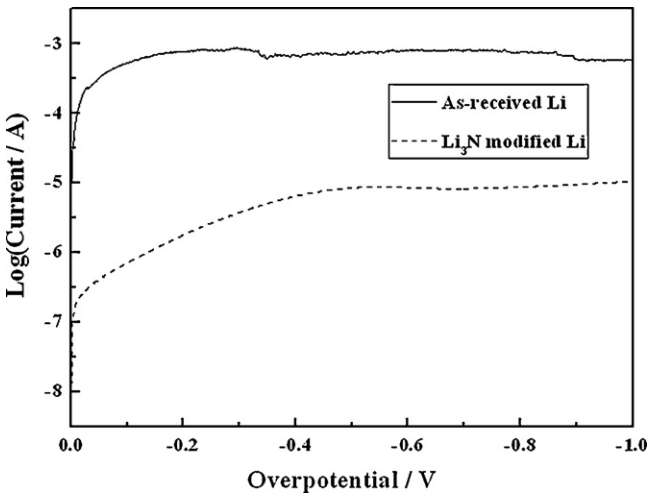

Fig. 5. Cathodic polarization (Tafel) curves of the Li as received and Li_3N (1 h) modified Li electrodes.

where ω is the angular frequency in rad s^{-1}, Y_0 is the magnitude of O which can be approximately converted into a 'Warburg' impedance and $B = l/D^{1/2}$, where l is the length of a stagnant layer and D is diffusion coefficient. According to the studies of Chang and Jong [31], the diffusion coefficient of Li^+ in the electrolyte is about 3.4×10^{-6} cm^2 s^{-1}. The length of a stagnant layer can therefore be calculated.

The fitted results of the impedance spectra in Fig. 4a and b are given in Tables 1 and 2, respectively. The goodness of fit for the whole electrode system is represented by the Chi-square (χ^2) parameter. Comparing R_f and Q_f in two tables, it is demonstrated that the SEI film formed on Li_3N modified Li electrode surface is smoother and less resistive. As Li_3N protective film is formed previously and used as the closest layer to Li metal, it can effectively prevent the side reactions between Li and electrolyte. Also, the highest Li ion conductivity of Li_3N among inorganic Li salts provides much smaller Li^+ migration resistance R_f. It is noticeable that the larger values Y_0 of 'Cothyperbol' element O and shorter lengths of stagnant layers suggest faster Li^+ diffusion from electrolyte to Li surface, owing to fewer reduction species in the electrolyte with Li_3N modification.

3.2.2. Kinetic performance analysis

To test polarization behavior is a promising technique to study the kinetic performance of electrodes [32,33]. Fig. 5 shows the cathodic polarization (Tafel) curves of the as-received Li and Li_3N (1 h) modified Li electrodes measured in $LiPF_6$/EC + DMC electrolyte. According to Tafel formulate written as Eq. (4):

$$\eta = \left(\frac{2.3RT}{\alpha nF}\right) lg \;\; i_0 - \left(\frac{2.3RT}{\alpha nF}\right) lg \;\; i \qquad (4)$$

where η is the overpotential of the electrode, n is the electronic stoichiometric number of electrode reaction, R is molar gas constant, T is room temperature (298 K), α is the transmission coefficient of electrode reaction, F is Faraday constant, i_0 is exchange current, the two important parameters (α, i_0) of kinetic performance can be calculated from Tafel slop and intercept. The results are shown in

Table 1
Fitting results obtained from the equivalent circuit of Fig. 4a.

Time (h)	L (10^{-7} H)	R_s (Ω)	Q_f (Y_{0f}, n) (10^{-5} S^n Ω^{-1})	R_f (Ω)	O (Y_0, B) (10^{-2} S^n Ω^{-1}, $s^{-1/2}$)	l (10^{-3} cm)	χ^2
1	2.163	1.887	4.979, 0.6824	363	0.3870, 1.822	3.457	0.1836
24	2.136	2.221	5.294, 0.6690	589	0.2731, 2.439	4.628	0.2784
48	2.317	1.443	5.292, 0.6674	594	0.2431, 2.464	4.675	0.3298
72	1.994	2.871	5.120, 0.6686	615	0.2386, 2.459	4.665	0.2844

Table 2
Fitting results obtained from the equivalent circuit of Fig. 4b.

Time (h)	L (10^{-7} H)	R_s (Ω)	Q_f (Y_{0f}, n) (10^{-5} S^n Ω^{-1})	R_f (Ω)	O (Y_0, B) (10^{-2} S^n Ω^{-1}, $s^{-1/2}$)	l (10^{-3} cm)	χ^2
1	1.769	2.435	3.920, 0.7282	98.6	8.693, 1.815	3.444	0.0404
24	2.299	1.808	1.889, 0.7648	331	0.9496, 1.498	3.842	0.0966
48	9.314	9.47	1.544, 0.7887	326	0.8583, 1.339	2.541	0.7777
72	4.09	4.09	1.899, 0.7614	379	0.8929, 1.497	2.840	0.0564

Table 3
Calculated results from Tafel curves of primitive Li andLi_3N (1 h) modified Li electrodes.

	Exchange current, i_0 (A)	Transition coefficient, α
Premitive Li electrode	2.789×10^{-4}	0.1583
Li_3N modified Li electrode	2.642×10^{-7}	0.2524

Table 3. As the active energy of Li ion reduction is expressed by the Eq. (5):

$$E_1 = E_0 + \alpha nF\eta \quad (5)$$

where E_0 is the active energy of reduction process without polarization. The higher value α of Li_3N modified Li electrode suggests higher active energy of Li ion charge transfer. It indicates that Li_3N modification has greatly decreased the reactivity of Li surface. However, the increased charge transfer resistance does not affect electrode reaction rate as Li^+ migration through the surface film is the rate-determining step for the whole reduction process [34]. Compared with as-received Li, a lower exchange current of 3.244×10^{-7} A suggests a complete SEI film is formed at the Li_3N modified Li electrode|electrolyte interface.

3.2.3. Cycling performance analysis

Typical cyclic voltammograms for Li deposition and dissolution on the Cu substrate surface are given in Fig. 6. As expected, the reduction of Li^+ to Li occurs at near 0 V. A small current loop characteristic of an overpotential-driven nucleation/growth electrodeposition process [35] is observed in 0 to −0.09 V region of both voltammograms. A larger cathodic overpotential is needed for the as-received Li electrode to initiate the nucleation and subsequent growth of Li deposits, indicating that a thick and resistive passive film is formed on the Li surface. The more negative potential of the as-received Li results in more insoluble reduction species precipitated on the Cu substrate surface, such as insoluble Li halides, LiOH–Li_2O and $ROCO_2Li$ [36]. So two dissolution peaks are observed in curve (a). The first dissolution peak at round 0.2 V must be due to the oxidation of the bulk Li deposits because it is close to the thermodynamic redox potential of Li. The second dissolution peak at ca. 0.4 V can be attributed to the stripping of reduction species, which are precipitated on the Cu substrate surface upon polarizing to more negative potential. In curve (b), the re-oxidation of Li deposits on the Cu substrate gives a single dissolution peak, indicating fewer side reactions between Li_3N modified Li electrode and electrolyte. And the smaller maximum deposition current of curve (b), which relates to diffusion limitations, suggests faster Li^+ migration between two electrodes.

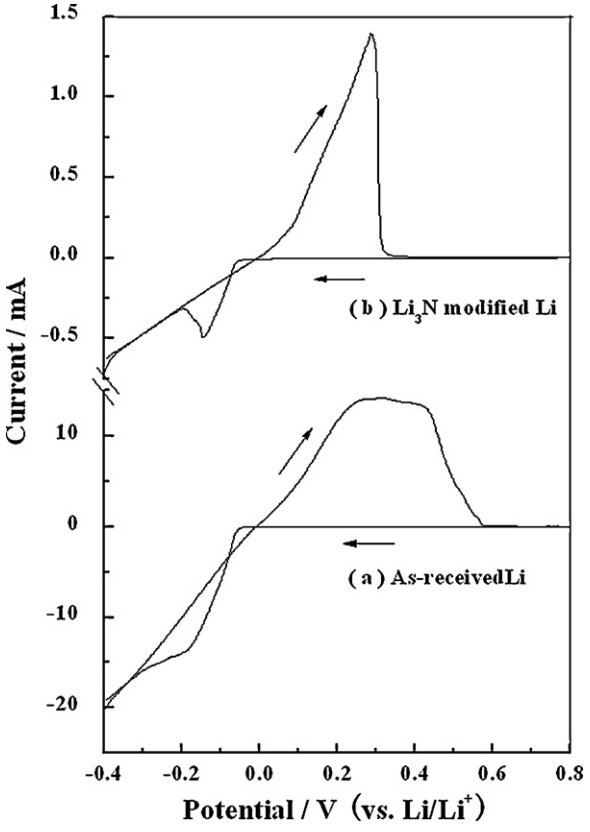

Fig. 6. Cyclic voltammograms for Li deposition and dissolution in 1 M $LiPF_6$/EC + DMC electrolyte with the Li as received (a) and Li_3N (1 h) modified Li (b) as counter electrodes.

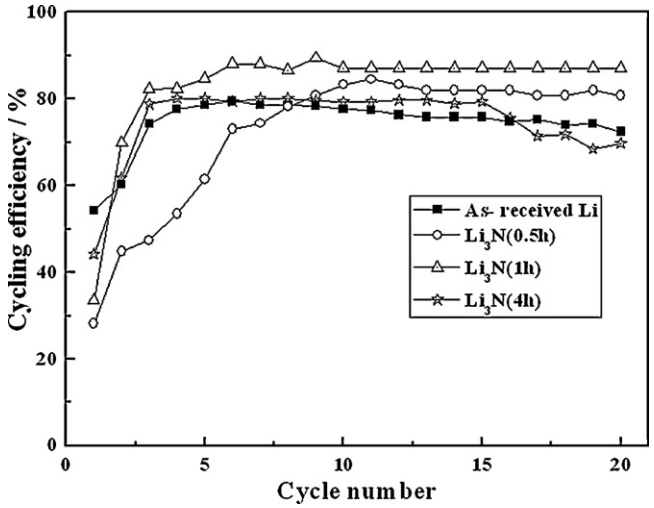

Fig. 7. Li cycling efficiency for the first 20 charge/discharge cycles with different N_2 exposing times, (■) primitive Li; (○) Li_3N (0.5 h); (△) Li_3N (1 h); (☆) Li_3N (4 h).

Fig. 7 shows the Li cycling efficiency for the first 20 charge/discharge cycles with different N_2 exposing times. As seen, the improvement of Li cycling efficiency depends on the N_2 exposing time. Neither short exposing time (0.5 h) nor long exposing time (4 h) affects the Li cycling efficiency obviously. Fig. 8 shows the Li cycling efficiency of the as received and the Li_3N (1 h) modified lithium electrodes in $LiPF_6$/EC + DMC electrolyte for 100 cycles. The modification increased the cycling efficiency by about 15%

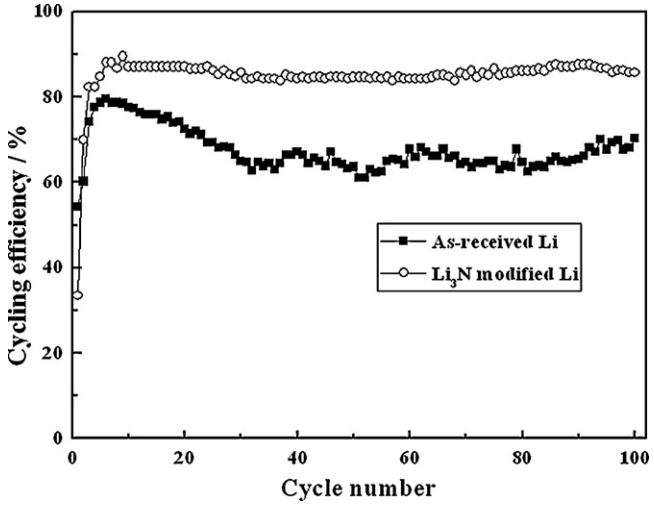

Fig. 8. Variation of Li cycling efficiency vs. cycle number without (■) and with Li_3N (1 h) (○) modification in 1 M $LiPF_6$/EC + DMC electrolyte for 100 cycles.

after 30 cycles, indicating that a proper exposing time is important to establish a high quality modified surface. However, both first cycling efficiencies are low, probably due to surface oxides on the Cu substrate, which may produce a Li_2O layer before Li deposition [37]. Meantime, an obvious fluctuation of the efficiency of the as-received Li after five cycles is observed due to the deposition of non-uniform and insoluble Li salts on the Cu substrate, which is also demonstrated in cyclic voltammetry measurements.

In order to find out whether the Li_3N film is broken or not during the charge/discharge cycling, the AC impedance tests of symmetrical cells with Li_3N modified Li electrodes were carried out after the cells were charged and discharged under the same conditions as those of the Cu/Li cells. The AC impedance results for symmetrical cells after different charge/discharge cycles were shown in Fig. 9. The interface resistance of Li_3N modified Li after 100 cycles is almost the same as that before cycling and has increased only about 10 Ω after 185 cycles, indicating that the interface is stable. So it can be concluded that Li_3N film is durable at least for 100 cycles. But for practical use, more precisely investigation is still needed.

The morphologies of the as-received Li and Li_3N modified Li electrodes before and after 100 charge/discharge cycles are given in Fig. 10. As seen in Fig. 10a and b, both electrode surfaces are inhomogeneous before cycling. It is noticeable that the modified surface is strongly charged by the electron beam since the Li_3N film is electronically insulated. However, the uneven native surface does not obviously affect the morphologies of Li deposits, as would be expected from non-uniform distribution of current. Most and all of Li deposits observed in Fig. 10c and d, respectively, are all in uniform 'particle-shape' after 100 charge/discharge cycles. According to the overpotential-driven nucleation/growth electrodeposition mechanism for Li reduction process, the uniform Li deposits should depend on the uniformity of the composition, structure and electrical properties of the surface film. It means that the morphology of Li deposits is primarily controlled by the components of the surface film and not at all by the initial topography of the surface (shape edges, "hill", steep corners, etc.). And Li_3N modification provides a complete SEI film at the interface. Therefore, the Li nucleus can continuously grow beneath the protective film, whereas relatively porous film on the as-received Li electrode surface leads to further growth of Li deposits out of the surface film, which is identified by the big Li agglomerates on Li surface shown in Fig. 10c.

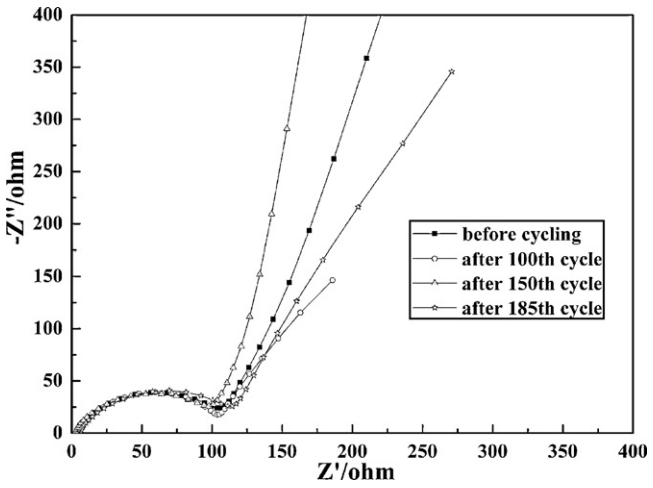

Fig. 9. AC impedance of symmetrical cells using Li_3N (1 h) modified Li electrodes after different charge/discharge cycles.

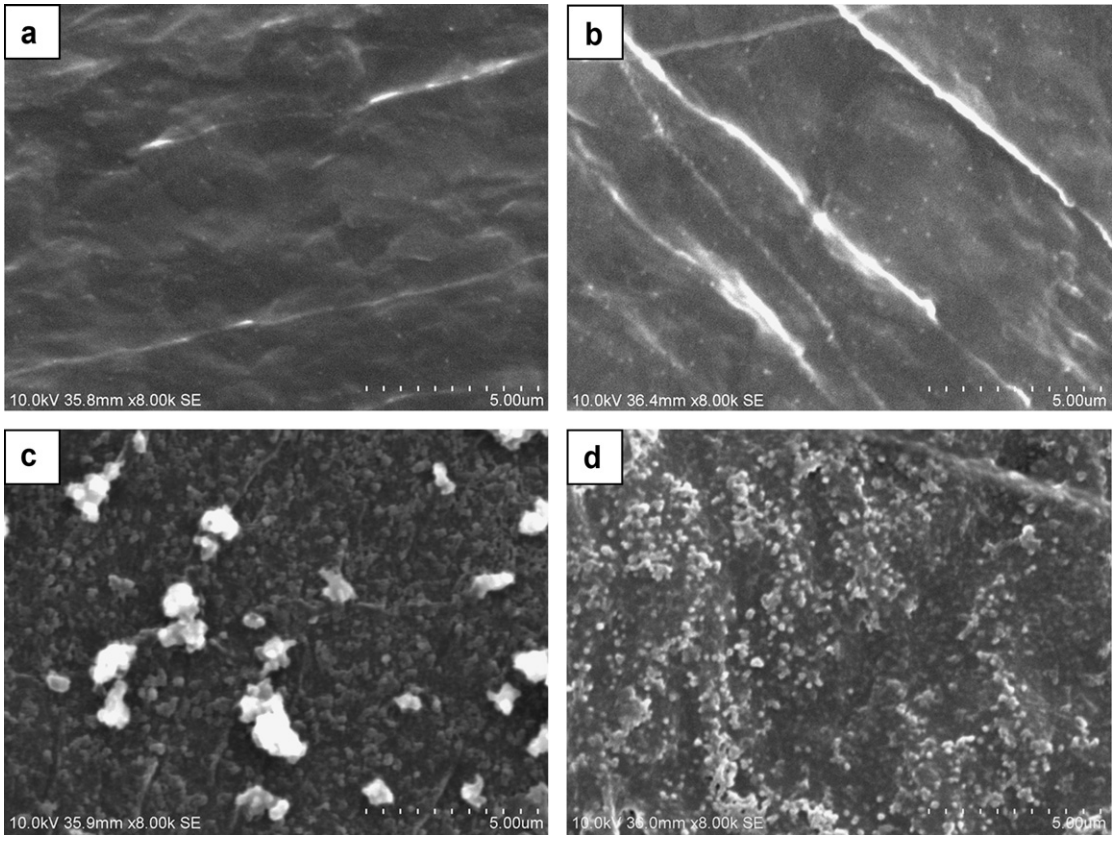

Fig. 10. SEM micrographs of the Li as received and Li_3N modified Li electrodes before (a and b) and after 100 charge/discharge cycles (c and d).

4. Conclusions

A Li_3N film is formed by reacting Li with N_2 gas at room temperature. The Li_3N modified Li electrode shows high stability in the electrolyte compared with the as-received Li electrode. Moreover, the extremely small exchange current demonstrates a complete SEI film formed at the electrode|electrolyte interface. The resistance of Li^+ migration through the surface film and the length of Li ion diffusion from electrolyte to electrode surface are significantly decreased by the modification. The Li cycling efficiency depends on the N_2 exposing time and is enhanced by Li_3N (1 h) modification. Moreover, the Li_3N film is durable for at least 100 charge/discharge cycles.

Acknowledgements

This work was financially supported by the Natural Science Foundation of China (NSFC, Project No. 50973127) and a 973 project of China No. 2007CB209700 as well as the Science and Technology Commission of Shanghai Municipality (projects no. 08DZ2210900 and no. 09PJ1410800).

References

[1] H. Ota, Y. Sakata, Y. Otake, K. Shima, M. Ue, J.-I. Yamaki, J. Electrochem. Soc. 151 (2004) A1778–A1788.
[2] E. Pled, J. Electrochem. Soc. 126 (1979) 2047–2051.
[3] R.D. Rauch, S.B. Brummer, Electrochim. Acta 22 (1977) 75–83.
[4] S. Tobishima, M. Arakawa, H. Hirai, J. Yamaki, J. Power Sources 26 (1989) 449–454.
[5] D. Aurbach, Y. Gofer, Y. Langzam, J. Electrochem. Soc. 136 (1989) 3198–3205.
[6] D. Aurbach, Y. Gofer, J. Electrochem. Soc. 138 (1991) 3529–3536.
[7] M. Arakawa, Y. Nemoto, S. Tobishima, M. Ichimura, J. Yamaki, J. Power Sources 43 (1993) 27–35.
[8] J.O. Besenhard, J. Gürtler, P. Komenda, A. Paxinos, J. Power Sources 20 (1987) 253–258.
[9] I. Yoshimatsu, T. Hirai, J. Yamaki, J. Electrochem. Soc. 135 (1988) 2422–2427.
[10] K. Kanamura, S. Shiraishi, Z. Takehara, J. Electrochem. Soc. 141 (1994) L108–L110.
[11] K. Kanamura, S. Shiraishi, Z. Takehara, J. Electrochem. Soc. 143 (1996) 2187–2197.
[12] S. Shiraishi, K. Kanamura, Z. Takehara, Langmuir 13 (1997) 3542–3549.
[13] Z. Takehara, J. Power Sources 68 (1997) 82–86.
[14] Y.S. Fung, H.C. Lal, J. Appl. Electrochem. 22 (1992) 255–261.
[15] J.O. Besenhard, J. Yangm, M. Winter, J. Power Sources 68 (1997) 87–90.
[16] M. Ishikawa, M. Morita, Y. Matsuda, J. Power Sources 68 (1997) 501–505.
[17] M. Morita, S. Aoki, Y. Matsuda, Electrochim. Acta 31 (1992) 119–123.
[18] K.M. Abraham, J.S. Foos, J.L. Goldman, J. Electrochem. Soc. 131 (1984) 2197–2199.
[19] N.J. Dudney, J. Power Sources 89 (2000) 176–179.
[20] L.C. Dejonghe, S.J. Visco, et al. US20080113261-A1.
[21] B.A. Boukamp, R.A. Huggins, Mater. Res. Bull. 13 (1978) 23–32.
[22] Y. Yan, J.Y. Zhang, et al., Eur. Phys. J. B 61 (2008) 397–403.
[23] S.X. Cui, et al., Solid State Commun. 149 (2009) 612–615.
[24] C.N. Cao, Q.J. Zhang, et al., Introduction in Electrochemistry Impedance Spectroscopy, Science Publication, China, 2002, pp. 25.
[25] D. Aurbach, A. Zaban, J. Electroanal. Chem. 367 (1994) 15–25.
[26] D. Aurbach, I. Weismann, O. Chusid, A. Zaban, Electrochim. Acta 39 (1994) 51–71.
[27] A. Zaban, D. Aurbach, J. Power Sources 54 (1995) 289–295.
[28] D. Aurbach, et al., Langmuir 5 (1999) 2947–2960.
[29] C.H. Hsu, F. Mansfeld, Corrosion 57 (2001) 747–748.
[30] S. Frangini, S. Loreti, J. Power Sources 160 (2006) 800–804.
[31] Y.C. Chang, J.H. Jong, et al., J. Chin. Inst. Chem. Eng. 35 (2004) 425–432.
[32] J.S. Sakamoto, et al., Solid State Ionics 144 (3–4) (2001) 295–299.
[33] F. Ding, Study on Lithium Metal Anode Material of High Specific Energy Lithium Secondary Battery[D], Harbin Institute of Technology, Harbin (China), 2006.
[34] D. Aurbach, Y. Cohen, J. Electrochem. Soc. 144 (1997) 3355–3360.
[35] R. Greef, R. Peat, L.M. Peter, D. Pletcher, J. Robinson, Instrumental Methods in Electrochemistry, Ellis Horwood, Chichester, 1985, pp. 211.
[36] D. Aurbach, Y. Cohen, J. Electrochem. Soc. 143 (1996) 3525–3532.
[37] T. Osaka, T. Momma, et al., J. Power Sources 68 (1997) 497–500.